Nuclear Instruments and Methods in Physics Research B 283 (2012) 29–34

Contents lists available at SciVerse ScienceDirect

Nuclear Instruments and Methods in Physics Research B

journal homepage: www.elsevier.com/locate/nimb

Axial ion channeling patterns from ultra-thin silicon membranes

M. Motapothula [a,*], Z.Y. Dang [a], T. Venkatesan [b], M.B.H. Breese [a,c], M.A. Rana [d], A. Osman [e]

[a] Center for Ion Beam Applications, Physics Department, National University of Singapore, Lower Kent Ridge Road, Singapore 117542, Singapore
[b] NanoCore, National University of Singapore, Singapore 117576, Singapore
[c] SSLS, National University of Singapore, 5 Research Link, Singapore 117603, Singapore
[d] Physics Division, Directorate of Science, PINSTECH, P.O. Nilore, Islamabad, Pakistan
[e] National Centre for Physics (NCP), Shahdara Valley Road, Islamabad, Pakistan

ARTICLE INFO

Article history:
Received 19 December 2011
Received in revised form 5 April 2012
Available online 11 April 2012

Keywords:
Transmission axial channeling
MeV protons
Silicon
FLUX simulation

ABSTRACT

We present channeling patterns produced by MeV protons transmitted through 55 nm thick [001] silicon membranes showing the early evolution of the axially channeled beam angular distribution for small tilts away from the [001], [011] and [111] axes. Instead of a ring-like "doughnut" distribution previously observed at small tilts to major axes in thicker membranes, geometric shapes such as squares and hexagons are observed along different axes in ultra-thin membranes. The different shapes arise because of the highly non-equilibrium transverse momentum distribution of the channeled beam during its initial propagation in the crystal and the reduced multiple scattering which allows the fine angular structure to be resolved. We describe a simple geometric construction of the intersecting planar channels at an axis to gain insight into the origin of the geometric shapes observed in such patterns and how they evolve into the 'doughnut' distributions in thicker crystals.

1. Introduction

Axial and planar ion channeling effects are important across a wide energy spectrum [1,2] from keV energies for ion implantation, MeV energies for ion beam analysis [3,4], and GeV to TeV energies for proton beam extraction experiments [5,6]. Channeling occurs when the transverse energy of an incident ion is less than the continuum potential energy of an atomic row or plane in a single crystal. Using the continuum approximation Lindhard and Selsk [7] derived the critical angle ψ_a for axial channeling and ψ_p for planar channeling to occur for ions incident on a crystal at small angles to a major axis or plane. Barrett [8,9] developed a numerical approach using an ion-atom scattering approach, which was able to simulate axial and planar channeling oscillations in thin crystals and to calculate the nuclear encounter probability around an axis. Ions incident at tilts slightly greater than the critical angle may be strongly scattered with high energy loss as they travel close to the atomic rows or planes, producing shoulders in angular dips and exclusion or 'blocking' of ions from the plane or axis [10].

The trajectories of ions incident close to axial alignment are dominated by the axial potential since it is several times larger than the planar potentials of the corresponding planes which intersect it. There is an angular range of about $0.1\psi_a$ over which ions may be 'hyperchanneled', where their trajectories are confined within a single axial channel and exhibit lower energy loss than most axially channeled ions which freely wander from one channel to another. Appleton et al. [11] measured the angular distribution of energy losses of 21.6 MeV iodine ions along the [011] axis of a 600 nm thick gold crystal and observed low energy losses of hyperchanneled ions, and high energy losses at small axial tilts, attributed to the beam aligned with the shoulders of widest planes.

A study of the angular distributions produced by 3.2 MeV protons at small [011] axial tilts in silicon crystals of 200–300 nm thickness reported ring-like 'doughnut' distributions for axial tilts in the range of $0.5\ \psi_a$–ψ_a. For a small axial tilt the beam has transverse momentum relative to the axis. As the ions oscillate during their trajectories through the crystal they acquire a wide range of possible azimuthal angles with similar magnitude of transverse momentum, resulting in a ring-like distribution in the projected channeling pattern. These were observed to be concentric with the [011] axis with a diameter proportional to the tilt and an azimuthal intensity which peaked at the intersections of the widest planes [12], indicating that the ions are also influenced by the planar potentials of the intersecting planes.

More recently, axial channeling in thin membranes was studied to characterize the effects of 'rainbow' channeling [13–16] which predicts a singular differential transmission cross-section and the formation of fine structure such as points and ridges of width about $0.02\psi_a$ in the angular distribution through very thin crystals. The predicted change in angular shape of the axially channeled rainbow distribution from a square to a diamond shape was observed [15] using MeV carbon ions and protons in a 1480 nm thick silicon [001] crystal. There have been several simulation studies of

* Corresponding author. Tel.: +65 83086250; fax: +65 67776126.
E-mail address: g0801315@nus.edu.sg (M. Motapothula).

0168-583X/$ - see front matter © 2012 Elsevier B.V. All rights reserved.
http://dx.doi.org/10.1016/j.nimb.2012.04.006

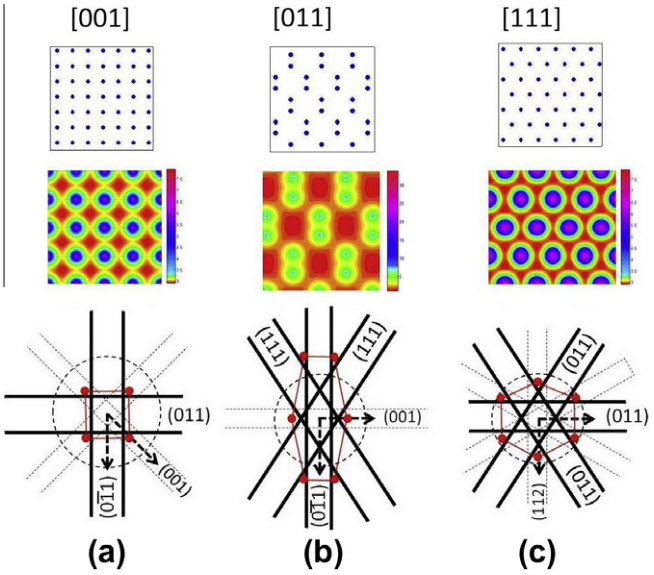

Fig. 1. Schematic of the shoulders of the widest intersecting planes at the [001], [011] and [111] axes. The width of the planes and axes are based on their respectively critical angles. The wider {011} and {111} planes are shown in bold lines whereas the narrower {001} and {112} planes are shown faintly. The tilt directions are shown by the dashed arrows. The shape outlines shown in red lines are formed by connecting the locations where the shoulders of widest planes intersect. (For interpretation of the references to colour in this figure legend, the reader is referred to the web version of this article.)

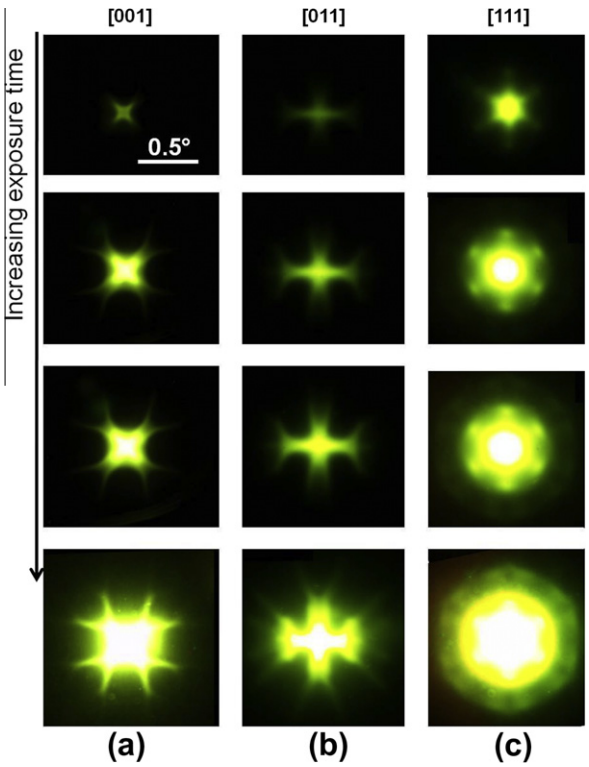

Fig. 2. Experimental channeling patterns for 2 MeV protons from a 55 nm [001] Si membrane at alignment with the (a) [001], (b) [011] and (c) [111] axes. Downwards direction shows the effect of increasing camera exposure.

ion channeling patterns produced by MeV ions passing through 200–300 nm thick silicon membranes [17,18] and ultra-thin silicon membranes of about 100 nm [13,16,19,20] for small tilts away from a major crystal axis or plane, mainly with the aim of

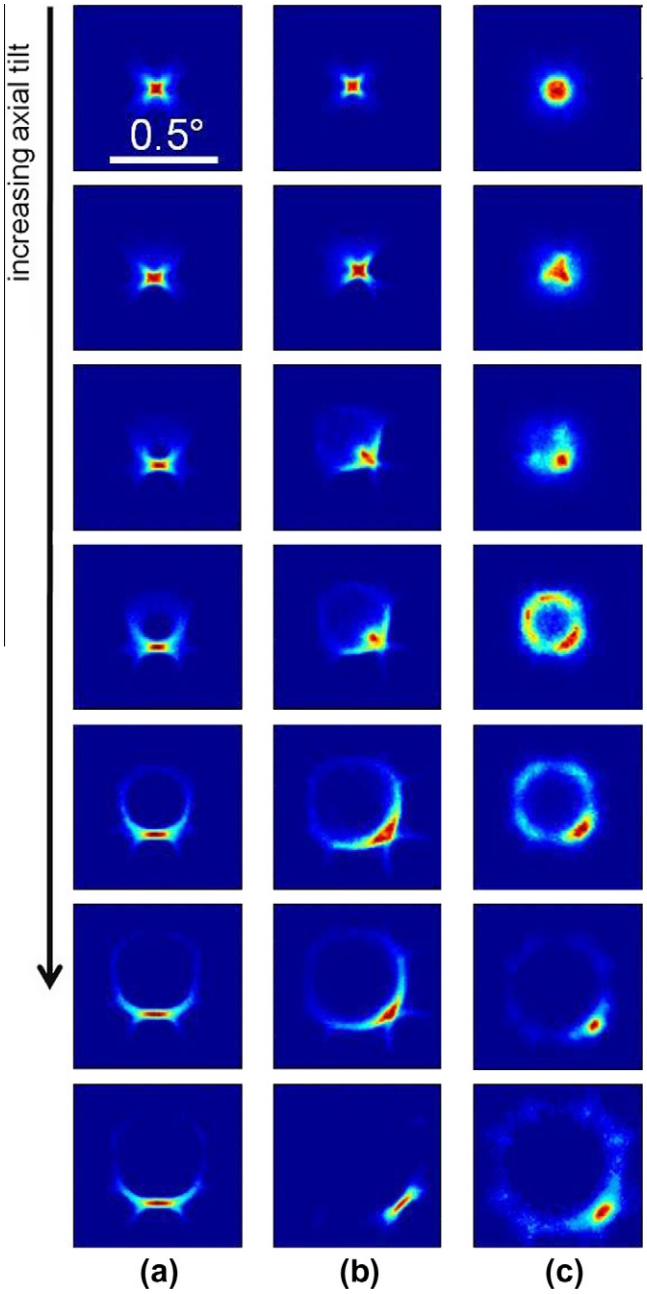

Fig. 3. FLUX simulations for the angular distributions of 2 MeV protons transmitted through a silicon [001] membrane for increasing tilt away from the axis in increments of $\psi_a/6$. The membrane thickness and tilt planes are: (a) 55 nm (0$\bar{1}$1), (b) 55 nm (001) and (c) 220 nm (001).

understanding rainbow channeling behavior. However, in all such experimental studies of ion channeling patterns in thin crystals [12,14,15,17] the minimum achievable membrane thickness was 140 nm though a more typical thickness was 200 nm, prepared as described in Section 2. In passing through 80 nm thick silicon layer along {011} plane 2 MeV proton beam acquires a full-width-at-half-maximum (FWHM) angular spread of about 0.012° [19]. For 2 MeV protons in silicon, ψ_a [001] = 0.33°, so multiple scattering limits the observable angular resolution to about $\sim 0.04\psi_a$ in this example. It was therefore not possible to experimentally observe the early evolution of an axially channeled ion beam distribution in crystal membranes which are sufficiently thin so that multiple scattering does not significantly degrade any fine angular structure, so none of these simulated patterns have been observed.

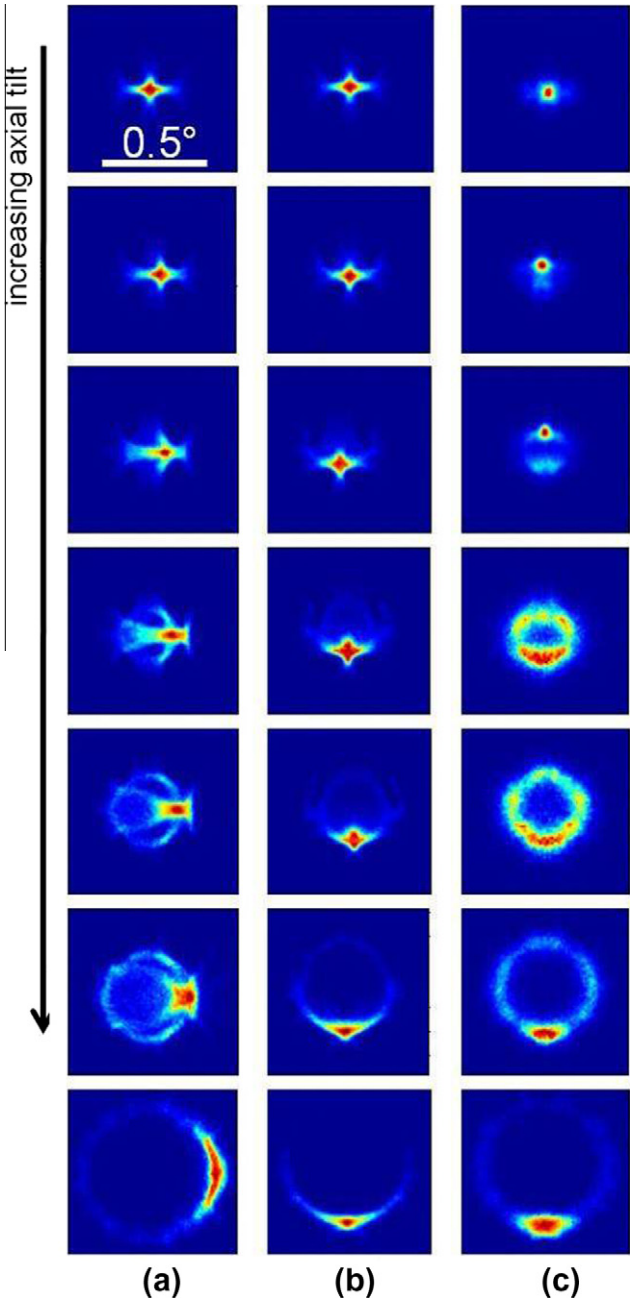

Fig. 4. FLUX simulations for the angular distributions of 2 MeV protons transmitted through a silicon [011] membrane for increasing tilt away from the axis in increments of $\psi_a/6$. The membrane thickness and tilt planes are: (a) 80 nm (001), (b) 80 nm ($0\bar{1}1$), (c) 300 nm ($0\bar{1}1$).

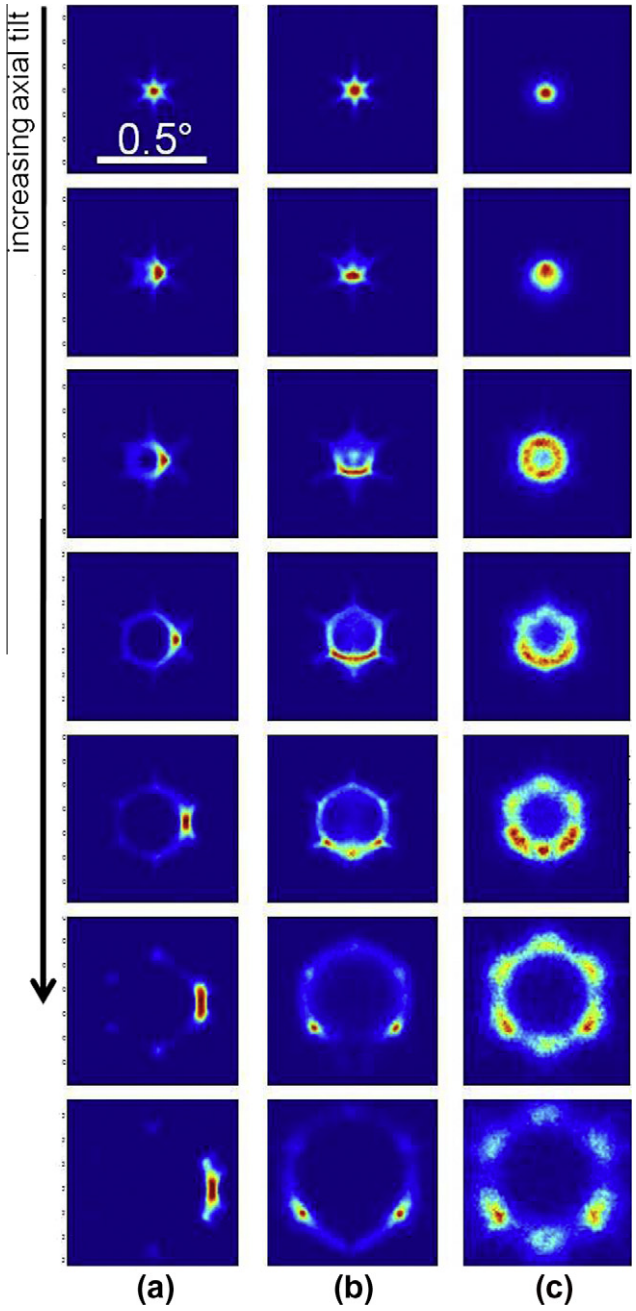

Fig. 5. FLUX simulations for the angular distributions of 2 MeV protons transmitted through a silicon [111] membrane for increasing tilt away from the axis in increments of $\psi_a/6$. The membrane thickness and tilt planes are: (a) 80 nm (011) (b) 80 nm (112) and (c) 300 nm (112).

Fabrication and characterization of ultra-thin silicon membranes which are suitable for observing ion channeling patterns using a focused MeV proton beam was recently reported [22] and used to study the different channeling behavior observed at wide and narrow {111} planes, and asymmetric behavior at axes containing a {111} plane [23]. Despite previous theoretical and simulation studies of channeling through ultra-thin layers [18–20], there are no systematic results allowing for an easy comparison of the expected behavior along each major axes under identical conditions. Therefore in Section 3, Monte Carlo simulations of channeling patterns produced by 2 MeV protons at small tilts to the [001], [011] and [111] axes are presented along with experimental patterns recorded along each axis using 55 nm membranes. Section 4 discusses the origin of the geometric shapes observed along each axis in these ultra-thin membranes using a simple geometric construction of the intersecting widest planes, and describes new features observed in such channeling patterns.

2. Simulated and experimental ion channeling patterns through ultra-thin membranes

Fig. 1 shows the orientations and tilt directions away from the [001], [011] and [111] axes for the simulated and experimental patterns presented here. For 2 MeV protons, the axial channeling critical angles are ψ [011] = 0.41° and ψ [111] = 0.36°, and the relevant planar critical angles are $\psi_{\{001\}} = 0.14°$, $\psi_{\{011\}} = 0.18°$,

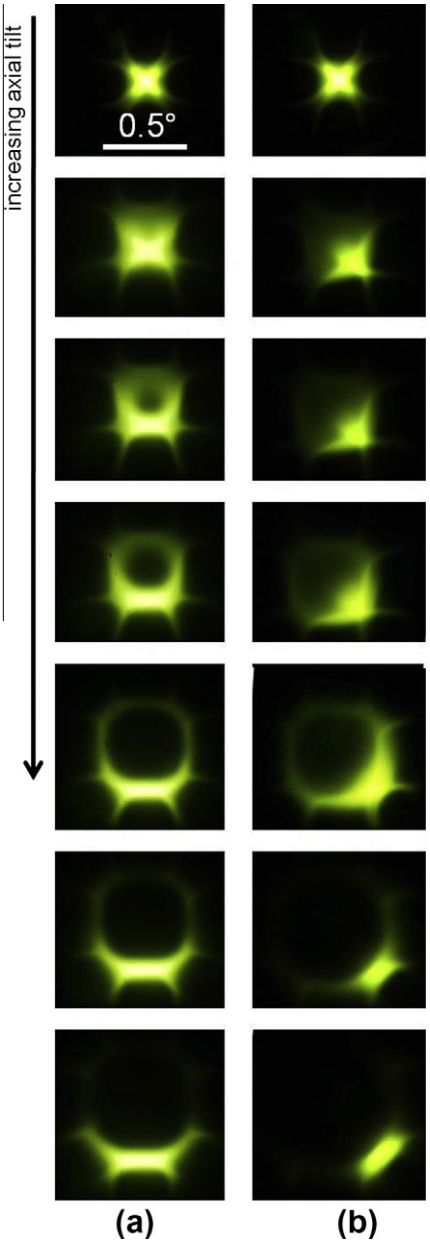

Fig. 6. Experimental channeling patterns for 2 MeV protons from a 55 nm [001] Si membrane for increasing tilts away from the [001] axis in increments of $\psi_a/6$. The tilt planes are: (a) $(0\bar{1}1)$ and (b) (001).

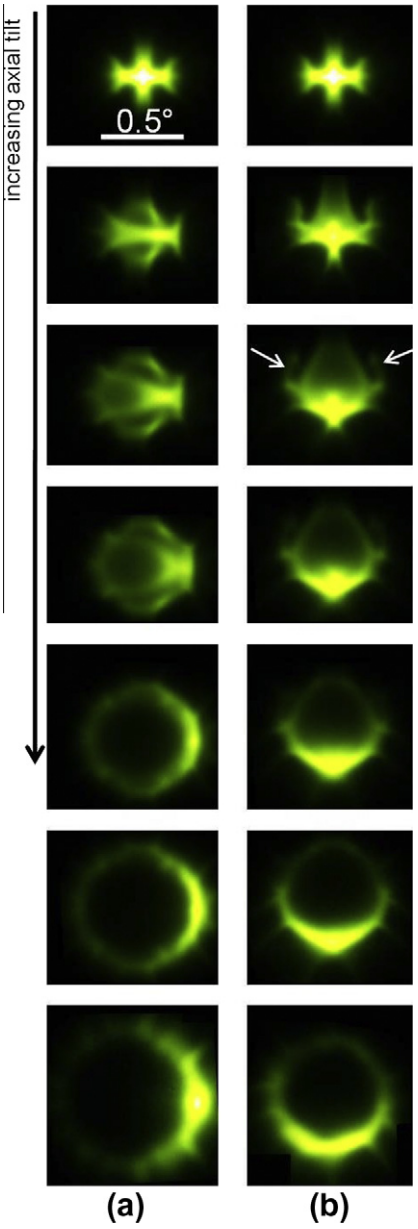

Fig. 7. Experimental channeling patterns for 2 MeV protons from a 55 nm [001] Si membrane for increasing tilts away from the [011] axis in increments of $\psi_a/6$. The tilt planes are: (a) $(0\bar{1}1)$ and (b) $(0\bar{1}1)$.

$\psi_{\{111\}} = 0.20°$ and $\psi_{\{112\}} = 0.11°$. The shape outlines shown by red lines and dots in Fig. 1 are discussed in Section 3.

Before presenting patterns produced on tilting away from each axis, Fig. 2 shows experimental patterns recorded at axial alignment along all three major axes as the camera exposure time is progressively increased. At the lowest exposure the observed patterns are in good agreement with those predicted by rainbow channeling theory [14,16,19,20]. A more detailed study on our observations of rainbow channeling phenomena in ultra-thin membranes at axial alignment will be published separately and are not further discussed here. As the exposure is increased the central axial regions become saturated and fainter regions where beam is scattered over a larger angular extent outside the axial potential are observed. One may consider these patterns as showing the different probabilities of beam being scattered along certain directions outside the axial potential, as determined by the interaction of different intersecting planes. Away from the [001] axis, the intersections of the {001} and {011} planes is observed (one is arrowed). Away from the [011] axis more complex intersections of the {001}, {111} and {011} planes produces a large number of lines radiating away from the axis. Both these examples occur because the scattered beam is still trapped within the intersecting planar potential, and cannot scatter into a random alignment.

The [111] axis displays a different effect. At a moderate exposure, one observes six separated outer dots (one is arrowed), forming a concentric pattern about the [111] axis. The slightly blurred appearance of these patterns, particularly those for long exposure, is a real effect, not an artifact of the recording system, as verified by observing the doughnuts at the same exposure time can be seen from Fig. 7, discussed below.

The Monte Carlo channeling code FLUX [24,25] which uses the Ziegler–Biersack–Littmark universal potential, and a binary collision model with an impact parameter dependent algorithm for en-

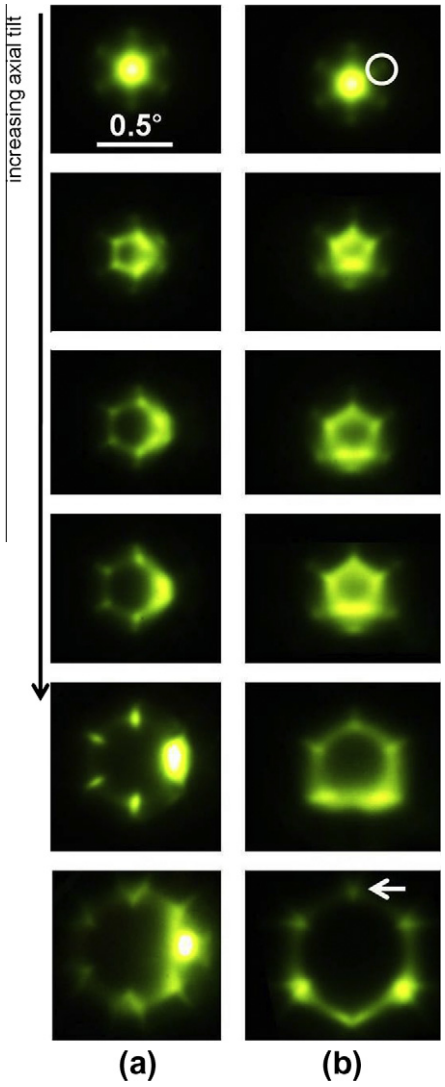

Fig. 8. Experimental channeling patterns for 2 MeV protons from a 55 nm [001] Si membrane for increasing tilts away from the [111] axis in increments of $\psi_a/6$. The tilt planes are: (a) (011) and (b) (112).

ergy loss was used to simulate channeled proton trajectories under the same conditions as used to record the experimental patterns. Figs. 3–5 show simulations of the exit angular distribution of 40,000 2 MeV protons transmitted through silicon membranes close to the [001], [011] and [111] axes respectively, for increasing tilt away from the axis. The top of each column shows the pattern at axial alignment and the bottom of each column shows the pattern at a tilt of ψ_a. In each figure, column (c) corresponds to simulated patterns through a thick membrane. These provide a comparison with the simulated patterns through ultra-thin layers in columns (a), (b) for a layer thickness of 55 nm for the [001] axis and 80 nm for the [011] and [111] axes. These thicknesses are based on the experimental geometry where the 55 nm thick membrane is tilted through 45° to the [011] and 54.7° for the [111] axes, giving a path length of about 80 nm.

For each axis, tilts along two directions, indicated by dashed arrows in Fig. 1, are simulated to study the range of different patterns produced at each axis. Fig. 3 shows patterns for tilts away from the [001] axis within the (a) vertically-running $(0\bar{1}1)$ planes and (b) the (001) planes. Fig. 4 shows patterns for tilts away from the [011] axis within the (a) horizontally-running (001) planes and (b) vertically-running $(0\bar{1}1)$ planes. Fig. 5 presents patterns for

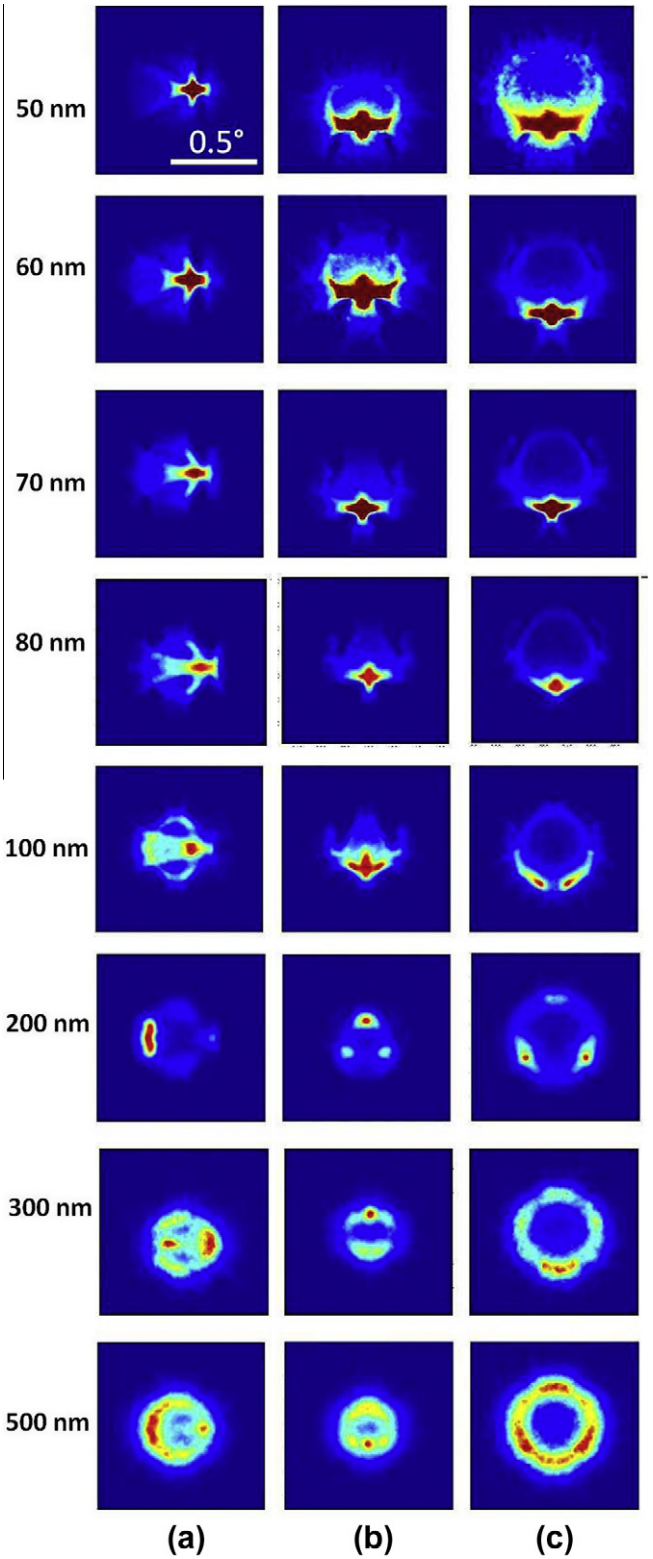

Fig. 9. FLUX simulations for the angular distributions of 2 MeV protons transmitted through a silicon [011] membrane for increasing membrane thickness, for tilts away from the [011] axis of (a) (001) planes, 0.10°, (b) $(0\bar{1}1)$ planes, 0.12° (c) $(0\bar{1}1)$ planes, 0.18°.

tilts away from the [111] axis within the (a) horizontally-running (011) planes and (b) vertically-running (112) planes. The tilt directions in columns (b), (c) of each figure are the same to compare the effects of a change in layer thickness on the patterns.

Figs. 6–8 show experimental channeling patterns for 2 MeV protons transmitted through a 55 nm thick silicon membrane around the [001], [011] and [111] axes respectively. The patterns were recorded by photographing a highly sensitive aluminum-coated YAG scintillator screen located 50 cm downstream of the membrane, using a beam current of about 10 pA with a beam convergence angle of $\Phi \sim 0.01°$, and a camera exposure time of 0.8 s. The tilt directions are the same as those in columns (a), (b) of Figs. 2–4.

3. Discussion

Comparing the simulated and experimental patterns for small tilts along each axis in ultra-thin membranes, similar characteristic features are observed. Faint portions are better resolved in the experimental patterns since one can saturate the more intense portions of the patterns when required, and one is not limited by counting statistics as in the simulated patterns. The experimental results thus provide a validation of the fine structure observed in the simulations. The characteristic feature of the [001] patterns is the formation of a square shape for small tilts. This is clearly observed in both simulated and experimental patterns along the (001) direction, and also in the experimental patterns along the $(0\bar{1}1)$ direction but only faintly in the corresponding $(0\bar{1}1)$ simulated patterns. Ref. [21] attributes the absence of blocking in Fig. 6b at incident angles less than the critical angle, as being where the axially channeled protons emerge in the center of the doughnut corresponding to trajectories which were changing their direction at the point of emergence from the crystal due to surface transmission (or) exit lattice inter atomic potential. The characteristic features of the [011] patterns on tilting along the horizontally-running (001) direction is the formation of a double ring-like structure, and for tilting along the vertically-running $(0\bar{1}1)$ direction is the formation of a half elongated hexagon with separated outer arms. These arms are arrowed in the experimental patterns where they are very distinct and also in the corresponding simulations where they are much fainter. The characteristic features of the [111] patterns for tilts along the vertically-running (112) direction is the crown-like distribution at small tilts which evolves into a perfect hexagon at larger tilts.

The simulated patterns observed through thick layers in Figs. 3c–5c all exhibit ring-like, 'doughnut' distributions for axial tilts over a wide tilt range of $\sim 0.5\ \psi_a$–ψ_a. In comparison, in ultra-thin membranes, 'doughnut' distributions are observed only over a narrow range of tilts around $\sim\psi_a$. In thin and thick membranes, peaks of the 'doughnut' distributions are located at azimuthal angles corresponding to the intersections of the widest planes [12]. This is clearly shown in the bottom simulation in Fig. 5c for tilting about the [111] axis where six distinct peaks at these locations are clearly observed. The origin of these peaks can be seen from the bottom experimental pattern of Fig. 8b, where these angular regions exhibit intense, sharply-resolved V-shaped grooves (one is arrowed) as a result of blocking at the intersecting planar shoulders. In Fig. 1 the intersections of the widest planar shoulders are indicated by dots. A square shape (outline shown in red) is formed around the [001] axis by these dots at the intersections of the orthogonal {011} planes. For the [011] axis, the shape formed by the dots at the intersections of the {011} and {111} planes is a hexagon elongated along the vertical axis. Similarly along the [111] axis, a perfect hexagon is formed.

These geometric shapes and their azimuthal orientation in the schematic in Fig. 1 agree well with those observed in experiments and simulations along the [001] and [111] axes. There is also agreement with the elongated hexagonal shape observed at the [011] axis for tilts along the $(0\bar{1}1)$ direction, though not with the double-ring shape for tilts along the (001) direction. We conclude that the widest intersecting planar shoulders not only modulate the azimuthal angular intensity of the beam projected close to a particular axis, as already observed in thicker crystals, but in ultra-thin membranes the shape of the projected angular distribution is a direct reflection of them. This is not observed in thicker crystals owing to additional multiple scattering which blurs the fine angular structure.

The simulations in Fig. 8 show the range of layer thicknesses over which the geometric shapes close to the [011] axis are observed for a fixed tilt angle. On tilting along the horizontally-running (001) direction, Fig. 9a, the formation and subsequent disappearance of the double structure occurs within the first 100 nm, with a more regular doughnut pattern observed in thicker layers. For tilting along the vertically-running $(0\bar{1}1)$ direction, Fig. 9b and c, the half-elongated hexagon and separated outer arms shapes also form and then disappear within the first 100 nm, with a more regular doughnut pattern produced in thicker layers.

4. Conclusions

We have recorded experimental channeling patterns along the three major axes, all of which are in good agreement with simulated results. In such ultra-thin membranes, the channeling patterns exhibit geometric shapes which, in most cases, are a reflection of that formed by their widest intersecting planes. Considering this work in conjunction with that of Appleton et al. [11] who considered the angular limits of the axial hyperchanneling regime, we conclude that a consideration of the effects of the widest intersecting planes is useful in understanding several aspects of axial ion channeling.

References

[1] D.V. Morgan (Ed.), Channeling, Theory, Observation and Applications, Wiley, London, 1973.
[2] D. Gemmell, Rev. Mod. Phys. 46 (1974) 129.
[3] L.C. Feldman, J.W. Mayer, S.T. Picraux, Materials Analysis by Ion Channeling, Academic Press, New York, 1982.
[4] M.B.H. Breese, P.J.C. King, P.J.M. Smulders, G.W. Grime, Phys. Rev. B 51 (1995) 2742.
[5] V.M. Biryukov, Yu.A. Chesnokov, V.I. Kotov, Crystal Channeling and its Application at High Energy Accelerators, Springer, Berlin, 1997.
[6] R.A. Carrigan Jr. et al., Phys. Rev. ST AB 1 (1998) 022801.
[7] J. Lindhard, K.Dan.Vidensk. Selsk, Mat.-Fys. Medd. 34 (14) (1965).
[8] J.H. Barrett, Phys. Rev. 166 (1968) 219.
[9] J.H. Barrett, Phys. Rev. B 3 (1971) 1527.
[10] D.S. Gemmell, R.E. Holland, Phys. Rev. Lett. 14 (1965) 945.
[11] B.R. Appleton, C.D. Moak, T.S. Noggle, J.H. Barrett, Phys. Rev. Lett. 28 (1972) 1307.
[12] J.S. Rosner, W.M. Gibson, J.A. Golovchenko, A.N. Goland, H.E. Wegner, Phys. Rev. B 18 (1978) 1066.
[13] N. Neškovic, Phys. Rev. B 33 (1986) 6030.
[14] H.F. Krause, S. Datz, P.F. Dittner, J. Gomez del Campo, P.D. Miller, C.D. Moak, N. Neskovic, P.L. Pepmiller, Phys. Rev. B 33 (1986) 6036.
[15] H.F. Krause, J.H. Barrett, S. Datz, P.F. Dittner, N.L. Jones, J. Gomez del Campo, C.R. Vane, Phys. Rev. A 49 (1994) 283.
[16] S. Petrovic, L. Miletic, N. Neskovic, Phys. Rev. B 61 (2000) 184.
[17] M.B.H. Breese, P.J.C. King, G.W. Grime, P.J.M. Smulders, L.E. Seiberling, M.A. Boshart, Phys. Rev. B 53 (1996) 8267.
[18] M.B.H. Breese, D.G. de Kerckhove, P.J.M. Smulders, D.N. Jamieson, Nucl. Instr. Meth. B 159 (1999) 248.
[19] D. Borka, S.N. Petrović, N. Nešković, J. Elect, Spec. Rel. Phenom. 129 (2003) 183.
[20] N. Nešković, S. Petrović, D. Borka, S. Kossionides, Phys. Letts. A 304 (2002) 114.
[21] D.D. Armstrong, W.M. Gibson, H.E. Wegner, Radiat Eff. 11 (1971) 241–249.
[22] Z.Y. Dang, M. Motapothula, Y.S. Ow, T. Venkatesan, M.B.H. Breese, M.A. Rana, A. Osman, APL 99 (2011), http://dx.doi.org/10.1063/1.3665620.
[23] M. Motapothula, Z.Y. Dang, T. Venkatesan, M.B.H. Breese, M.A. Rana, A. Osman, Phy. Rev. Lett. 108 (2012) 195502.
[24] P.J.M. Smulders, D.O. Boerma, Nucl. Instr. Meth. B 29 (1987) 471.
[25] P.J.M. Smulders, D.O. Boerma, M. Shaanan, Nucl. Instr. Meth. B 45 (1990) 450.